Superconductor Science and Technology

PAPER • OPEN ACCESS

Anisotropic monoblock model for computing AC loss in partially coupled Roebel cables

OPEN ACCESS
IOP Publishing
Superconductor Science and Technology
Supercond. Sci. Technol. **33** (2020) 094013 (8pp)
https://doi.org/10.1088/1361-6668/ab9939

Anisotropic monoblock model for computing AC loss in partially coupled Roebel cables

Simon Otten[1,2], Anna Kario[1,2], Eduard Demenčik[1], Rainer Nast[1] and Francesco Grilli[1]

[1] Karlsruhe Institute of Technology, Institute for Technical Physics, Hermann-von-Helmholtz-Platz 1, 76344 Eggenstein-Leopoldshafen, Germany
[2] University of Twente, Faculty of Science and Technology, Drienerlolaan 5, 7522NB Enschede, the Netherlands

E-mail: s.j.otten@utwente.nl

Received 1 February 2020, revised 15 April 2020
Accepted for publication 3 June 2020
Published 31 July 2020

Abstract

When exposed to time-dependent magnetic fields, REBCO Roebel cables generate AC loss resulting from both magnetic hysteresis and induced inter-strand coupling currents. Until now, the AC loss has been computed in a two-dimensional approximation assuming fully coupled or decoupled strands, and a finite inter-strand resistance could be simulated only with three-dimensional models. In this work, we propose a homogenization procedure that reduces the three-dimensional geometry of the Roebel cable to two dimensions, without ignoring connections between the strands. The homogenized cable consists of two parallel 'monoblocks' with an anisotropic resistivity. The proposed model enables computation of AC coupling loss without the need for complex three-dimensional simulations. For experimental validation, a Roebel cable with soldered strands was prepared. The inter-strand resistance was determined by applying a transverse current and measuring the voltage profile. Additionally, the AC magnetization loss of the cable was measured in fields of 1 to 50 mT with frequencies of 1 to 2048 Hz using a calibration-free technique. With the measured inter-strand resistance as input parameter, the monoblock model gives a good estimate for the AC loss, even for conditions in which the coupling loss is dominant.

Keywords: roebel cable, ac losses, coupling losses, hts coated conductors

(Some figures may appear in colour only in the online journal)

1. Introduction

The Roebel cable is a way to make fully transposed cables of REBCO coated conductors [1] (REBCO = rare-earth metal barium copper oxide). Short lengths of REBCO Roebel cable were first demonstrated by Karlsruhe Institute of Technology (KIT) [2] and Industrial Research ltd. (IRL) [3]. IRL later automatized the cable assembly process and developed methods for quality control [4, 5]. Roebel cables have been considered for use in high-field accelerator [6, 7] or fusion magnets [8], and also for power applications such as transformers [9, 10]. A unique property of REBCO Roebel cables is that the strands are transposed, but not twisted, and the anisotropic properties of coated conductors are retained. This enables magnet designs that exploit these anisotropic properties, such as 'aligned-block' coils, which use the maximum critical current density by aligning the conductor with the magnetic field [11]. The strands in REBCO Roebel cables are usually not insulated in order to create alternative paths for the current in

case of defects. A disadvantage is that a time-dependent magnetic field can induce inter-strand coupling currents, which lead to an increase in AC loss [12]. In order to predict the level of AC loss, electromagnetic modelling of Roebel cables is required. Several different approaches are already described in literature: often a cross-section of the Roebel cable is extended to infinity in order to reduce the problem from three to two dimensions [13–18]. More advanced three-dimensional models also exist [19–22]. However, none of these models take into account a finite resistance between the strands, and thus cannot predict coupling losses. A network model developed by van Nugteren *et al* simulates the three-dimensional cable taking into account coupling between the strands [23]. To our knowledge this is the only numerical model for Roebel cables that can predict AC coupling losses.

In this work, we aim to compute the magnetization AC loss in a Roebel cable with finite inter-strand resistance using a two-dimensional model, and evaluate it with an experiment. An approximation using a homogenization procedure is applied to evaluate the cable geometry in 2D including connections and interconnects between strands. This is done using a 'monoblock' model with anisotropic resistivity. The AC loss predicted by the monoblock model is compared to measurements on a cable with controlled inter-strand resistance. The magnetization AC loss is measured over a wide range of frequencies (1–2048 Hz) and amplitudes up to 50 mT. Due to limitations of the set-up, we have not been able to validate the model for higher amplitudes.

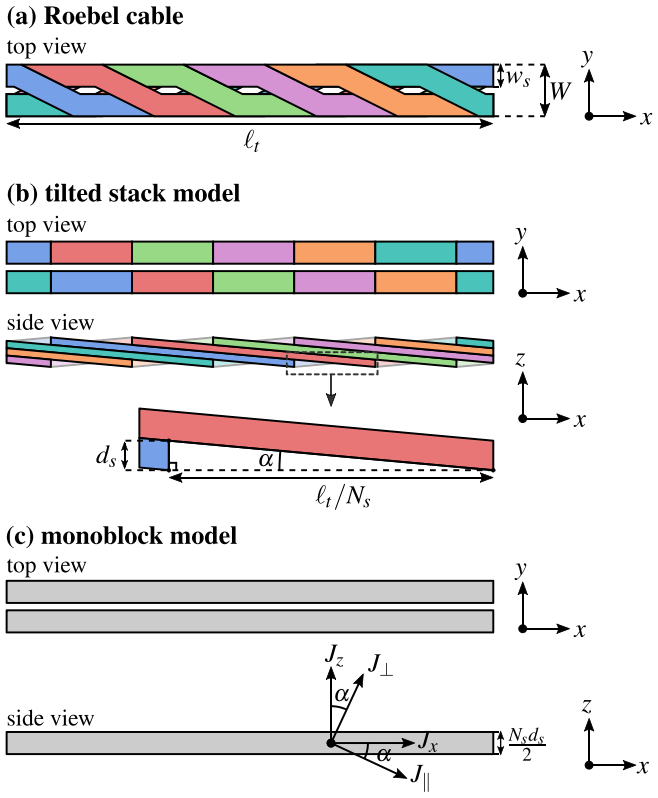

Figure 1. The simplification procedure for a Roebel cable with six strands.

2. Monoblock model

A Roebel cable is a complex three-dimensional structure. The aim is to simplify the cable to a two-dimensional geometry, without neglecting the influence of finite resistance between the strands. We consider a cable with N_s strands and a transposition length ℓ_t (see figure 1(a)). The strands have a thickness d_s and a width w_s. The width of the entire cable is given by W. The first step of the simplification is neglecting the influence of the cross-overs, where the strand go from one cable half to the other. The result is a 'tilted stack model', as shown in figure 1(b). Since the strands move up and down along the cable length, they have an angle with respect to the longitudinal x-direction. As seen from the sketch, this angle is given by:

$$\tan(\alpha) = \frac{N_s d_s}{\ell_t} \tag{1}$$

The second step is homogenizing the tilted stack into a uniform 'monoblock' (figure 1(c)). The monoblock is invariant in the x-direction, and thus a two-dimensional electromagnetic calculation in the yz-plane suffices. The monoblock has an anisotropic resistivity: In the direction parallel to the conductor, the block behaves as a superconductor, while perpendicular to the conductor the finite inter-strand resistance causes resistive behaviour. In general, the electric field and current density in the frame of the conductor are related by:

$$\begin{bmatrix} E_\parallel \\ E_\perp \end{bmatrix} = \begin{bmatrix} \rho_\parallel & 0 \\ 0 & \rho_\perp \end{bmatrix} \begin{bmatrix} J_\parallel \\ J_\perp \end{bmatrix} \tag{2}$$

where $E_\parallel, \rho_\parallel, J_\parallel$ and $E_\perp, \rho_\perp, J_\perp$ are the electric field, resistivity and current densities in the directions parallel and perpendicular to the conductor, respectively. The conductor frame is rotated with respect to xz-frame by an angle α in clockwise direction. The current densities in both frames are thus related by a rotation matrix:

$$\begin{bmatrix} J_\parallel \\ J_\perp \end{bmatrix} = \begin{bmatrix} \cos(\alpha) & -\sin(\alpha) \\ \sin(\alpha) & \cos(\alpha) \end{bmatrix} \begin{bmatrix} J_x \\ J_z \end{bmatrix} \tag{3}$$

In the same way one can find for the electric field:

$$\begin{bmatrix} E_x \\ E_z \end{bmatrix} = \begin{bmatrix} \cos(\alpha) & \sin(\alpha) \\ -\sin(\alpha) & \cos(\alpha) \end{bmatrix} \begin{bmatrix} E_\parallel \\ E_\perp \end{bmatrix} \tag{4}$$

Substitution of equations (2) and (3) into (4) results in the following $\boldsymbol{E}(\boldsymbol{J})$ relation in the xz-frame:

$$\begin{aligned} \begin{bmatrix} E_x \\ E_z \end{bmatrix} &= \begin{bmatrix} \cos(\alpha) & \sin(\alpha) \\ -\sin(\alpha) & \cos(\alpha) \end{bmatrix} \begin{bmatrix} \rho_\parallel & 0 \\ 0 & \rho_\perp \end{bmatrix} \\ &\quad \times \begin{bmatrix} \cos(\alpha) & -\sin(\alpha) \\ \sin(\alpha) & \cos(\alpha) \end{bmatrix} \begin{bmatrix} J_x \\ J_z \end{bmatrix} \\ &= \begin{bmatrix} \rho_\parallel \cos^2(\alpha) + \rho_\perp \sin^2(\alpha) & \left(\rho_\perp - \rho_\parallel\right) \sin(\alpha)\cos(\alpha) \\ \left(\rho_\perp - \rho_\parallel\right) \sin(\alpha)\cos(\alpha) & \rho_\perp \cos^2(\alpha) + \rho_\parallel \sin^2(\alpha) \end{bmatrix} \\ &\quad \times \begin{bmatrix} J_x \\ J_z \end{bmatrix} \end{aligned} \tag{5}$$

If $\rho_\parallel = \rho_\perp$, the diagonal entries of the resistivity matrix are equal and the off-diagonal elements of are zero, and thus

Ohm's law is retrieved.The perpendicular resistivity $\rho_\perp$ is a constant related to the inter-strand resistance, and can be experimentally determined. This will be discussed further in section 4.1. To simulate the behaviour of a superconductor, a non-linear power-law is used for the parallel resistivity:

$$\rho_\parallel = \frac{E_c}{|J_\parallel|}\left|\frac{J_\parallel}{J_c}\right|^n \tag{6}$$

In this equation, J_c is the critical current density of the monoblock, E_c is the electric field if $J_\parallel = J_c$, and n is a non-linearity index. The value of E_c needs to match the critical field used to determine J_c from measured IV-curves. We used a conventional value of $E_c = 10^{-4}$ V/m. Once the current distribution and electric field have been found, the power density can be obtained from the dot product:

$$p = \boldsymbol{E}\cdot\boldsymbol{J} = E_\parallel J_\parallel + E_\perp J_\perp \tag{7}$$

The first term is related to currents in the plane of the superconducting tape, and will be referred to as hysteresis loss. The second term results from currents between the strands and will be called coupling loss. The loss per cycle is found by integration of the power density over the monoblock cross-section and a full cycle of the magnetic field in time.

3. Numerical solution

3.1. Integral formulation

The monoblock model will now be used to compute the AC loss in a time-dependent but spatially uniform magnetic field perpendicular to the x-axis, assuming zero transport current. The current distribution is found numerically using an integral form of Maxwell's equations [24, 25]. The advantage of this formulation is that, unlike in a differential form, no boundary conditions are required, and the equations have to be solved only in the conductor volume. This makes the method convenient to implement for simple geometries such as the rectangular monoblock considered here. This section will give a short description of our implementation of the method, which is described in more detail in our previous publication [26].

The vector potential in the x-direction can be expressed as follows:

$$A(y,z,t) = A_{\text{ext}}(y,z,t) - \frac{\mu_0}{2\pi}\int_{-\infty}^{\infty}\int_{-\infty}^{\infty} \times \ln\left(\sqrt{(y-y')^2+(z-z')^2}\right) J(y',z',t)\mathrm{d}y'\mathrm{d}z' \tag{8}$$

In this equation, A_{ext} is a the vector potential related to the applied field and $J(y,z,t)$ is the current density in the x-direction. The conductor cross-section is divided in rectangular elements numbered $i = 1, 2, \ldots, N$, each carrying a uniform current density J_i (see figure 2). The vector potential can now be written as a sum:

$$A_i = A_{\text{ext},i} + \frac{\mu_0}{2\pi}\sum_{j=1}^{N} K_{ij}J_j \tag{9}$$

where the elements of K are given by

$$K_{ij} = -\int_{c_j}^{d_j}\int_{a_j}^{b_j} \ln\left(\sqrt{(y_i-y')^2+(z_i-z')^2}\right)\mathrm{d}y'\mathrm{d}z' \tag{10}$$

Element j is bounded by $a_j < y < b_j$, $c_j < z < d_j$ and (y_i, z_i) is a point in the center of element i. The expression for K can be evaluated by substituting $u = y_i - y'$, $v = z_i - z'$ and repeatedly integrating by parts:

$$K_{ij} = -\frac{1}{2}\left[\left[g(u,v)\right]_{u=y_i-a_j}^{y_i-b_j}\right]_{v=z_i-c_j}^{z_i-d_j} \tag{11}$$

$$g(u,v) = uv\left(\ln(u^2+v^2)-3\right) + u^2\tan^{-1}\left(\frac{v}{u}\right) + v^2\tan^{-1}\left(\frac{u}{v}\right) \tag{12}$$

As seen from figure 2, the problem is symmetric after a rotation of 180° around the x-axis. The rotation changes the sign of the magnetic field and thus the following relations hold:

$$\boldsymbol{B}(-y,-z,t) = -\boldsymbol{B}(y,z,t) \tag{13}$$

$$\boldsymbol{E}(-y,-z,t) = -\boldsymbol{E}(y,z,t) \tag{14}$$

$$\boldsymbol{J}(-y,-z,t) = -\boldsymbol{J}(y,z,t) \tag{15}$$

By taking advantage of this symmetry, only one half of the cable needs to be simulated. This reduces the number of unknowns by half and improves the computation time by rougly a factor four (see table 1). The matrix K taking into account the symmetry becomes:

$$K_{ij} = -\frac{1}{2}\left[\left[g(u,v)\right]_{u=y_i-a_j}^{y_i-b_j}\right]_{v=z_i-c_j}^{z_i-d_j} + \frac{1}{2}\left[\left[g(u,v)\right]_{u=y_i+b_j}^{y_i+a_j}\right]_{v=z_i+d_j}^{z_i+c_j} \tag{16}$$

Using the fact that $\partial\boldsymbol{A}/\partial t = -\boldsymbol{E} - \nabla\phi$ and assuming that the gradient of the electric potential $\nabla\phi$ is zero, equation (9) can be rewritten to:

$$\sum_{j=1}^{N} K_{ij}\frac{\partial J_j}{\partial t} = -\frac{2\pi}{\mu_0}\left(E_{x,i} + \frac{\partial A_{\text{ext},i}}{\partial t}\right) \tag{17}$$

This system of ordinary differential equations is numerically integrated to find the current distribution in time. For the simulations in this work, Matlab's built-in solver 'ode15s' was used [27].

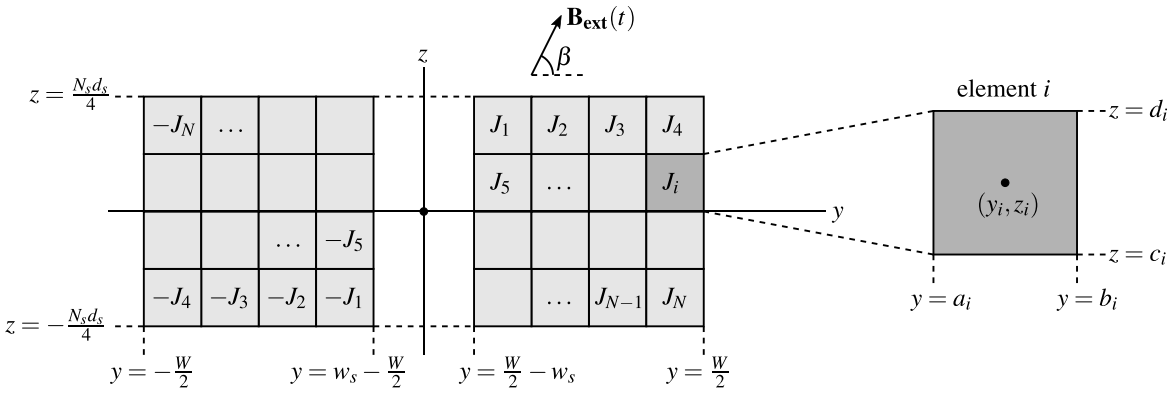

Figure 2. Division of the monoblock in rectangular elements with uniform current density. This figure shows a cross-sectional plane, to which the current flows perpendicular.

Table 1. Computation time for the full geometry (N = 800) or only one half exploiting symmetry (N = 400) with a 100 Hz applied field of different amplitudes (CPU: Intel Core i5-6500).

B_0 [mT]	time (full) [s]	time (half) [s]
1	8.4	2.4
2	11.9	3.5
5	19.9	5.4
10	28.7	8.0
20	42.8	11.0
50	64.2	17.4

3.2. Evaluation of the right-hand side of equation (17)

In order to evaluate the right-hand side of (17), the electric field must be computed from the current distribution. This is done using the anisotropic $\boldsymbol{E(J)}$ relation resulting from the monoblock model (equation (5)). A difficulty is that the monoblock model considers two components of the current, while the numerical approach solves for the x component only. To overcome this problem, inductive effects in the direction perpendicular to the conductor are neglected. In other words, it is assumed that transfer current between two strands is always homogeneously distributed over the width of the contact surface. The assumption makes it possible to eliminate the perpendicular current. However, it is not valid for very high frequencies at which skin effects influence the distribution of coupling currents. The effect on AC loss at such high frequencies will be discussed in further in section 4.3. From equation (3) we have:

$$J_\perp = \sin(\alpha)J_x + \cos(\alpha)J_z \tag{18}$$

By integration over the strand width we find:

$$\int_{y_1}^{y_2} J_\perp \mathrm{d}y = \sin(\alpha)\int_{y_1}^{y_2} J_x \mathrm{d}y + \cos(\alpha)\int_{y_1}^{y_2} J_z \mathrm{d}y \tag{19}$$

where $y_1 = \frac{W}{2} - w_s$ and $y_2 = \frac{W}{2}$. The first term is just $w_s J_\perp$ under the assumption of uniform current transfer. The third integral is zero because no net current can flow in the vertical direction. Therefore the perpendicular current is described by:

$$w_s J_\perp = \sin(\alpha)\int_{y_1}^{y_2} J_x \mathrm{d}y \tag{20}$$

By solving equation (18), J_z can now be expressed in terms of J_x:

$$\begin{aligned} J_z &= \frac{J_\perp - \sin(\alpha)J_x}{\cos(\alpha)} \\ &= \frac{1}{\cos(\alpha)}\left(\frac{\sin(\alpha)}{w_s}\int_{y_1}^{y_2} J_x \mathrm{d}y - \sin(\alpha)J_x\right) \\ &= -\tan(\alpha)\left(J_x - \frac{1}{w_s}\int_{y_1}^{y_2} J_x \mathrm{d}y\right) \end{aligned} \tag{21}$$

Now that J_z is known, E_x can be computed using equation (5):

$$E_x = \left(\rho_\parallel \cos^2(\alpha) + \rho_\perp \sin^2(\alpha)\right)J_x + \left(\rho_\perp - \rho_\parallel\right)\sin(\alpha)\cos(\alpha)J_z \tag{22}$$

The second term of the right-hand side of equation (17) is the external contribution to the vector potential. The external contribution is chosen to be:

$$\boldsymbol{A_{ext}}(y,z,t) = B_0 \sin(\omega t)\left(z\cos(\beta) - y\sin(\beta)\right)\hat{\boldsymbol{x}} \tag{23}$$

so that:

$$\boldsymbol{B_{ext}}(y,z,t) = \nabla \times \boldsymbol{A_{ext}} = B_0 \sin(\omega t)\left(\cos(\beta)\hat{\boldsymbol{y}} + \sin(\beta)\hat{\boldsymbol{z}}\right) \tag{24}$$

Thus β is the angle between the applied magnetic field and the y-axis. Note that this choice of $\boldsymbol{A_{ext}}$ respects the rotational symmetry and the invariance along x.

Table 2. Properties of the cable sample and derived quantities $\alpha, \rho_\perp$ and J_c used for the monoblock model.

Cable width	W	4.0	mm
Strand width	w_s	1.9	mm
Strand thickness	d_s	0.10	mm
Transposition length	ℓ_t	50	mm
Sample length	ℓ	150	mm
No. of strands	N_s	6	
Strand critical current	I_c	50.2	A
n-value	n	23.7	
Adjacent inter-strand resistance	ρ_a	0.265	$\mu\Omega$ m
Crossing inter-strand resistance	ρ_c	1.07	$\mu\Omega$ m
Conductor angle	α	0.012 0	rad
Perpendicular resistivity	$\rho_\perp$	4.04	$\mu\Omega$ m
Monoblock critical current density	J_c	264	A/mm^2

4. Experiment

4.1. Sample preparation

In order to study the effect of partial coupling more closely, we prepared a Roebel cable whose strands are soldered together. The cable properties are listed in table 2. A 4-mm-wide coated conductor manufactured by SuperPower (SCS4050-AP) was used. As specified by the manufacturer, this wire has a minimum self-field critical current of 109 A and an average of 111 A at 77 K. Six strands of 1.9 mm width were prepared by laser-cutting. A short transposition length of 50 mm was chosen so that three full transpositions could be measured in the limited sample area of the AC loss set-up. The critical current of the separate strands was measured in a liquid nitrogen bath (77 K). The average critical current was 50.2 ± 2.8 A and the n-value was 23.7 ± 1.4. The average critical current per unit width was 27.8 A/mm before and 26.4 A/mm after cutting, a decrease of 5%. The strands were then degreased and pre-soldered with In52Sn48 using rosin flux. The pre-soldered strands were then assembled into a cable, and the cable was once more heated to 170 °C under slight pressure to solder the strands together.

The monoblock critical current density was approximated by normalizing the strand critical current to the cross-sectional area which gives $J_c = 264$ A/mm^2. The field dependency of the critical current was not taken into account.

4.2. Inter-strand resistance

Roebel cables, like Rutherford cables, consist of a single layer of transposed strands. Even though the shape of the strands is very different, both cable types are topologically the same. Inter-strand connections in Rutherford cables are commonly described using a network model with two parameters [28–30], as shown in figure 3. R_c is the resistance at the point where a strand in the lower touches one in the upper layer. This connection occurs twice each transposition length for any pair of strands. A resistor of R_a connects adjacent strands and occurs $2N_s$ times in each transposition length. In order to adapt this inter-strand resistance network for the continuum model, we introduce length-averaged values for the resistance between adjacent and non-adjacent strands:

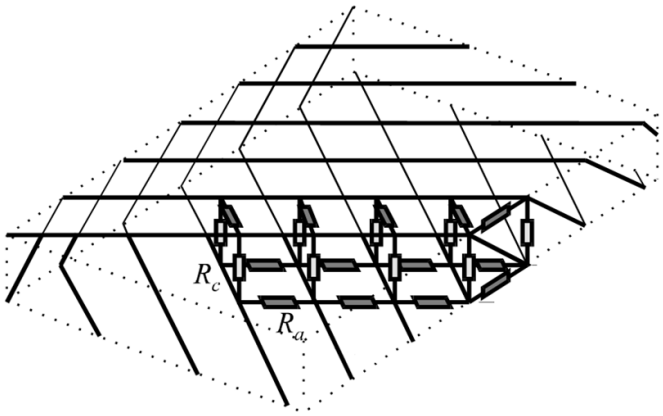

Figure 3. Inter-strand resistance model used for Rutherford cables. Image copied from [31] with permission from Arjan Verweij.

$$\rho_a = \frac{\ell_t}{2N_s} R_a \tag{25}$$

$$\rho_c = \frac{\ell_t}{2} R_c \tag{26}$$

Both quantities have units of Ω m. The resulting inter-strand resistance network for a cable of length ℓ is shown in figure 4.

The values of ρ_a and ρ_c were determined by applying a current between strand 3 and strand 6 and recording the voltage profile. This measurement was done at 77 K and therefore the strands were in the superconducting state. Because the applied current of 10 A is much lower than the critical current, the strands can be assumed to be equipotential planes. The strands can therefore be represented by the nodes of an electrical network, as shown in figure 4. By least-squares fitting of the network model to the measured voltage profile, inter-strand resistance values of $\rho_a = 0.265$ $\mu\Omega$ m and $\rho_c = 1.07$ $\mu\Omega$ m were found. The monoblock model considers current transfer between adjacent strands only. These are connected by ρ_a and ρ_c in parallel, thus the unit-length resistance between adjacent strands is $(1/\rho_a + 1/\rho_c)^{-1}$. By multiplying this value with the strands width w_s, the surface contact resistance is obtained. The perpendicular volume resistivity of the monoblock is found by multiplying this contact resistance with the number of contacts per unit length $1/d_s$.

$$\rho_\perp = \left(\frac{1}{\rho_a} + \frac{1}{\rho_c}\right)^{-1} \frac{w_s}{d_s} = 4.04\ \mu\Omega\text{m} \tag{27}$$

4.3. AC loss measurement

The AC loss per cycle in a sinusoidal field was measured at 77 K using a calibration-free technique [32]. The applied magnetic field was uniform in space and perpendicular to the wide face of the cable ($\beta = 90°$). The measurements as well as the calculations using the monoblock model are shown in figure 5.

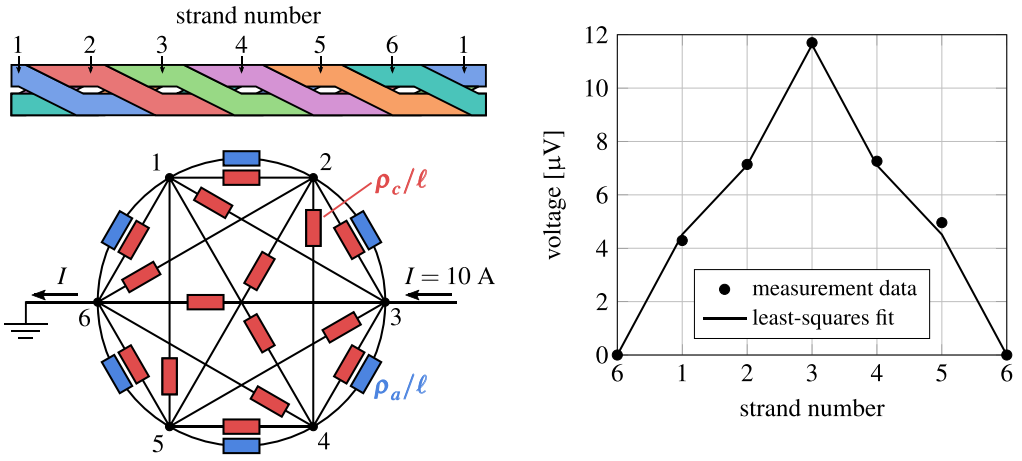

Figure 4. Inter-strand resistance measurement scheme (left) and result (right). The least-squares fit is found for $\rho_a = 0.265$ μΩ m and $\rho_c = 1.07$ μΩ m.

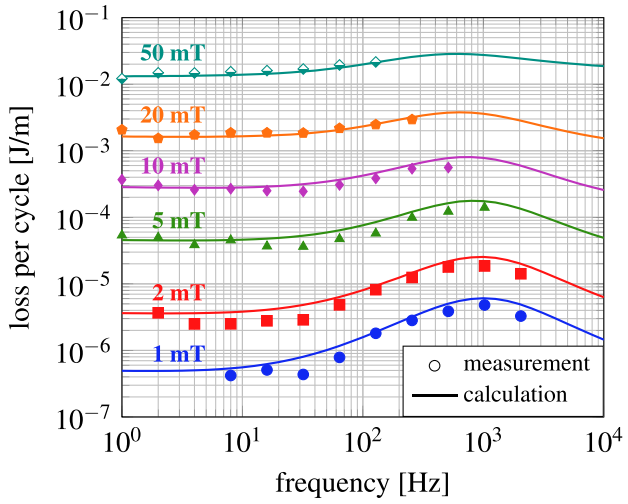

Figure 5. Measured and calculated AC loss of the soldered Roebel cable as a function of frequency and for field amplitudes ranging from 1 to 50 mT.

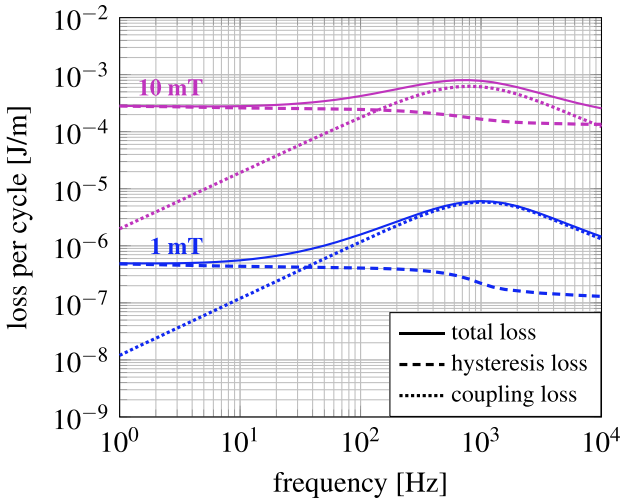

Figure 6. Contributions of hysteresis and coupling to the AC loss for field amplitudes of 1 and 10 mT.

Hysteresis loss is frequency independent according to the critical state model [33], although it can have a slight frequency dependence when a finite steepness of the transition is taken into account [34, 35]. Coupling currents are expected to have a stronger frequency dependence of the form $\omega l/(1+(\omega\tau)^2)$ [36], where τ is a decay time constant. To be able to detect the frequency dependent coupling loss, the measurement is done over a frequency range as wide as possible.

At the lowest amplitude of 1 mT, the AC loss increases by an order of magnitude as the frequency goes from 1 Hz to 1 kHz. This is seen in both the measurement and the calculation. Below penetration, the hysteresis losses are proportional to the third power of the magnetic field amplitude, while the coupling losses only increase with the amplitude squared. This explains the lower frequency dependence at higher amplitudes.

There is a reasonable agreement between calculation and measurement for frequencies up to 1 kHz. At higher frequencies, a decrease in AC loss is observed in both measured and predicted AC loss. Such a peak in AC loss of multifilamentary conductors can be explained using skin effect theory [37]. Due to limitations of the set-up, we could obtain only two measurement points at on the right side of the peak. The model could therefore not be adequately validated for these conditions.

In figure 6, the different contributions to the total loss can be seen in more detail. At the lowest frequencies ($f < 10$ Hz), the loss is dominated by hysteresis loss. The hysteresis loss has a very slight frequency dependence due to the finite n-value [34, 35]. The coupling loss increases linearly with frequency and becomes the dominant contribution for frequencies above roughly 100 Hz. At the highest frequencies, the coupling loss is limited by a skin effect [13]. We observe a remarkable drop of the hysteresis loss near 1 kHz. Above this frequency the strands become effectively coupled, which leads to lower hysteresis loss at field amplitudes below penetration

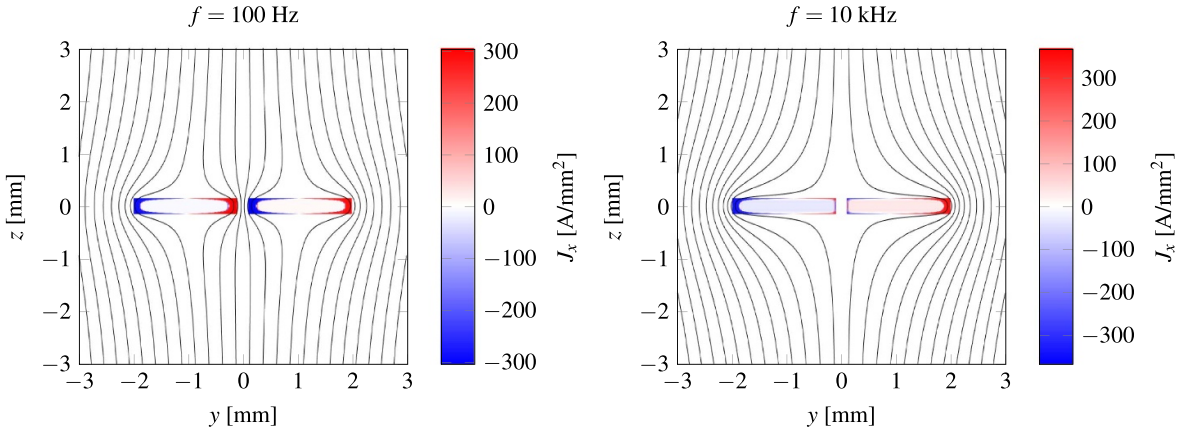

Figure 7. Current distribution and magnetic field lines at peak field ($B_0 = 10$ mT) at frequencies of 100 Hz and 10 kHz.

[14]. This effect is illustrated in figure 7, which shows the current distribution and magnetic field at frequencies of 100 Hz and 10 kHz. At 10 kHz, coupling currents shield the center from the external field. As a result, very little flux enters the superconductor from the cable center, and hysteresis loss is reduced.

5. Summary and outlook

The monoblock approximation reduces the three-dimensional cable geometry to much simpler two-dimensional problem. A finite resistance between strands can be introduced into the monoblock model by using an anisotropic resistivity. In this way, induced coupling currents and associated losses can be computed. We have used an integral formulation of Maxwell's equations to numerically solve the monoblock model.

A Roebel cable with soldered strands was prepared to validate the model. The inter-strand resistance was measured by applying a current between opposite strands and recording the voltage profile over all strands. From the measured inter-strand resistance, an equivalent perpendicular resistivity of the monoblock of $\rho_\perp = 4.04$ $\mu\Omega$m was found. The AC magnetization loss of the cable was measured using a calibration-free technique in magnetic fields amplitudes ranging from 1 to 50 mT. The measured loss had a reasonable agreement with the monoblock model for frequencies up to 1 kHz. Due to limitations of the set-up, it was not possible to validate the model at higher frequencies, at which the loss characteristic of the sample may be influenced by skin effects.

The approximation with a uniform but anisotropic material may be used as well for coupling loss calculations in other structures involving tilted stacks of coated conductors, such no-insulation racetrack or pancake coils. This will be the topic of a future investigation.

ORCID iD

Francesco Grilli https://orcid.org/0000-0003-0108-7235

References

[1] Goldacker W, Grilli F, Pardo E, Kario A, Schlachter S I and Vojenčiak M 2014 Roebel cables from REBCO coated conductors: a one-century-old concept for the superconductivity of the future *Supercond. Sci. Technol.* **27** 093001

[2] Goldacker W, Nast R, Kotzyba G, Schlachter S I, Frank A, Ringsdorf B, Schmidt C and Komarek P 2006 High current DyBCO-ROEBEL assembled coated conductor (RACC) *J. Phys.: Conf. Series* **43** 901–4

[3] Long N J, Badcock R, Beck P, Mulholl M, Ross N, Staines M, Sun H, Hamilton J and Buckley R G 2008 Narrow strand YBCO roebel cable for lowered AC loss *J. Phys.: Conf. Series* **97** 012280

[4] Badcock R A, Long N J, Mulholland M, Hellmann S, Wright A and Hamilton K A 2009 Progress in the manufacture of long length ybco roebel cables *IEEE Trans. Appl. Supercond.* **19** 3244–7

[5] Long N J, Badcock R A, Hamilton K, Wright A, Jiang Z and Lakshmi L S 2010 Development of YBCO roebel cables for high current transport and low AC loss applications *J. Phys.: Conf. Series* **234** 022021

[6] Rossi L *et al* 2015 The eucard-2 future magnets european collaboration for accelerator-quality hts magnets *IEEE Trans. Appl. Supercond.* **25** 4001007

[7] Lorin C *et al* 2015 Cos-theta design of dipole inserts made of rebco-roebel or bscco-rutherford cables *IEEE Trans. Appl. Supercond.* **25** 4000305

[8] Kario A, Vojenciak M, Grilli F, Kling A, Ringsdorf B, Walschburger U, Schlachter S I and Goldacker W 2013 Investigation of a rutherford cable using coated conductor roebel cables as strands *Supercond. Sci. Technol.* **26** 085019

[9] Glasson N, Staines M, Allpress N, Pannu M, Tanchon J, Pardo E, Badcock R and Buckley R 2017 Test results and conclusions from a 1 mva superconducting transformer featuring 2g hts roebel cable *IEEE Trans. Appl. Supercond.* **27** 5500205

[10] Fetisov S S *et al* 2016 Development and characterization of a 2g hts roebel cable for aircraft power systems *IEEE Trans. Appl. Supercond.* **26** 4803204

[11] van Nugteren J, Kirby G A, de Rijk G, Rossi L, Kate H H J and Dhallé M M J 2015 Study of a 5 t research dipole insert-magnet using an anisotropic rebco roebel cable *IEEE Trans. Appl. Supercond.* **25** 4000705 ten

[12] Lakshmi L S, Long N J, Badcock R A, Staines M P, Jiang Z, Thakur K P and Emhofer J 2011 Magnetic and transport ac losses in hts roebel cable *IEEE Trans. Appl. Supercond.* **21** 3311–15

[13] Terzieva S, Vojenčiak M, Pardo E, Grilli F, Drechsler A, Kling A, Kudymow A, Gömöry F and Goldacker W 2009 Transport and magnetization ac losses of ROEBEL assembled coated conductor cables: measurements and calculations *Supercond. Sci. Technol.* **23** 014023
[14] Grilli F and Pardo E 2010 Simulation of ac loss in roebel coated conductor cables *Supercond. Sci. Technol.* **23** 115018
[15] Thakur K P, Raj A, Brandt E H, Kvitkovic J and Pamidi S V 2011 Frequency-dependent critical current and transport ac loss of superconductor strip and roebel cable *Supercond. Sci. Technol.* **24** 065024
[16] Vojenčiak M, Grilli F, Terzieva S, Goldacker W, Kováčová M and Kling A 2011 Effect of self-field on the current distribution in roebel-assembled coated conductor cables *Supercond. Sci. Technol.* **24** 095002
[17] Grilli F, Zermeño V M and Kario A 2016 Designing hts roebel cables for low-field applications with open-source code *Phys. C: Supercond. Appl.* **530** 120–2
[18] Grilli F, Vojenčiak M, Kario A and Zermeño V 2016 Hts roebel cables: Self-field critical current and ac losses under simultaneous application of transport current and magnetic field *IEEE Trans. Appl. Supercond.* **26** 4803005
[19] Nii M, Amemiya N and Nakamura T 2012 Three-dimensional model for numerical electromagnetic field analyses of coated superconductors and its application to roebel cables *Supercond. Sci. Technol.* **25** 095011
[20] Zermeno V M R, Grilli F and Sirois F 2013 A full 3d time-dependent electromagnetic model for roebel cables *Supercond. Sci. Technol.* **26** 052001
[21] Amemiya N, Tsukamoto T, Nii M, Komeda T, Nakamura T *et al* 2014 Alternating current loss characteristics of a roebel cable consisting of coated conductors and a three-dimensional structure *Supercond. Sci. Technol.* **27** 035007
[22] Yan Y *et al* 2019 Experimental and numerical study on the magnetization process of roebel cable segments *IEEE Trans. Appl. Supercond.* **29** 8201005
[23] van Nugteren J *et al* 2016 Measurement and numerical evaluation of ac losses in a rebco roebel cable at 4.5 k *IEEE Trans. Appl. Supercond.* **26** 8201407
[24] Brandt E H 1994 Thin superconductors in a perpendicular magnetic ac field: General formulation and strip geometry *Phys. Rev.* B **49** 9024–40
[25] Brandt E H 1996 Superconductors of finite thickness in a perpendicular magnetic field: Strips and slabs *Phys. Rev.* B **54** 4246–64
[26] Otten S and Grilli F 2019 Simple and fast method for computing induced currents in superconductors using freely available solvers for ordinary differential equations *IEEE Trans. Appl. Supercond.* **29** 8202008
[27] Shampine L and Reichelt M 1997 The matlab ode suite *SIAM J. Sci. Comput.* **18** 1–22
[28] Sytnikov V, Svalov G, Akopov S and Peshkov I 1989 Coupling losses in superconducting transposed conductors located in changing magnetic fields *Cryogenics* **29** 926–30
[29] Verweij A P and ten Kate H H J 1993 Coupling currents in rutherford cables under time varying conditions *IEEE Trans. Appl. Supercond.* **3** 146–9
[30] Devred A, Bacquart L, Bredy P, Bruzek C E, Laumond Y, Otmani R and Schild T 1999 Interstrand resistance measurements on nb_3sn rutherford-type cables *IEEE Trans. Appl. Supercond.* **9** 722–6
[31] Verweij A 1995 Electrodynamics of superconducting cables in accelerator magnets *PhD thesis* University of Twente)
[32] Souc J, Gomory F and Vojenciak M 2005 Calibration free method for measurement of the ac magnetization loss *Supercond. Sci. Technol.* **18** 592
[33] Bean C P 1964 Magnetization of high-field superconductors *Rev. Mod. Phys.* **36** 31–9
[34] Sander M and Grilli F 2010 Fem-calculations on the frequency dependence of hysteretic losses in coated conductors *J. Phys.: Conf. Ser.* **234** 022030
[35] Polak M, Kvitkovic J, Mozola P, Usak E, Barnes P and Levin G 2007 Frequency dependence of hysteresis loss in ybco tapes *Supercond. Sci. Technol.* **20** S293
[36] Campbell A 1980 ac losses in cables of twisted multifilment superconductors *Cryogenics* **20** 651–4
[37] Kwasnitza K 1977 Scaling law for the ac losses of multifilament superconductors *Cryogenics* **17** 616–20